

In-Situ Fabrication of Polymeric Microcapsules by Ink-Jet Printing of Emulsions

*Renhua Deng**, *Yilin Wang*, *Lisong Yang* and *Colin D. Bain**

Department of Chemistry, Durham University, Stockton Road, Durham DH1 3LE, U.K.

KEYWORDS: ink-jet printing, microcapsules, polymer, emulsion, tebuconazole, phase separation

ABSTRACT: Phase separation driven by solvent evaporation of emulsions can be used to create polymeric microcapsules. The combination of emulsion solvent evaporation with ink-jet printing allows the rapid fabrication of polymeric microcapsules at a target location on a surface. The ink is an oil-in-water emulsion containing in the disperse phase a shell-forming polymer, a core-forming fluid that is a poor solvent for the polymer, and a low-boiling good solvent. After the emulsion is printed onto the substrate, the good solvent evaporates by diffusion through the aqueous phase and the polymer and poor solvent phase separate to form microcapsules. The continuous aqueous phase contains polyvinyl alcohol that serves as an emulsifier and as a binder of the capsules to the substrate. This method is demonstrated for microcapsules with various shell-forming polymers (PS, PMMA and PLLA) and core-forming poor solvents (hexadecane and a 4-heptanone/sunflower oil mixture). Cargoes such as fluorescent dyes (Nile Red and tetracyanoquinodimethane) or active ingredients (e.g. the fungicide tebuconazole) can be encapsulated. Uniform microcapsules are obtained by printing emulsions containing monodisperse

oil droplets produced in a microfluidic device. We discuss the physical parameters that need to be controlled for the successful fabrication of microcapsules in inkjet printing. The method for rapid, in-situ encapsulation could be useful for controlled-release applications including agrochemical sprays, fragrances, functional coatings and topical medicines.

Introduction

Polymeric microcapsules as containers/carriers can be used for self-healing coating,¹⁻³ sensors,^{4, 5} phase change materials,⁶ controlled release of drugs and pesticides,⁷⁻¹³ pressure-sensitive switches,¹⁴ displays or smart windows,^{15, 16} optical materials,¹⁷ enzyme immobilization,¹⁸ and fragrances¹⁹. Microcapsules can protect active cargoes against environmental hazards (such as moisture, oxidation and bacteria), and thus increase their shelf life.²⁰ Microcapsules allow the release of drugs in a controlled way,²¹⁻²⁸ which can enhance their efficacy and decreases costs and side effects. Moreover, encapsulation allowing the safe handling of toxic chemicals (such as pesticides) and permits liquid droplets to be handled as solids or to be embedded in a solid matrix.^{5.}

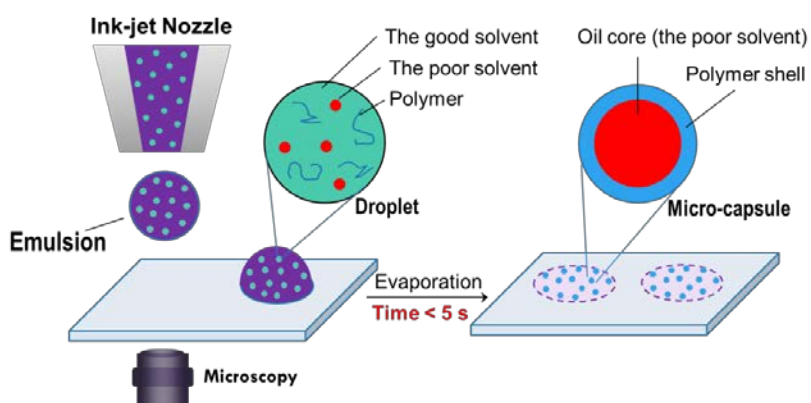
16

Various approaches for fabricating polymer microcapsules have been demonstrated,^{29, 30} including coacervation of polymers or polymerization at the interface of emulsion droplets,³¹ absorption of polymers or polymerization on the surface of solid templates (particles),⁸ evaporation of double emulsions,^{11, 21} and inner phase separation in emulsion droplets.³²⁻³⁴ Each method has limitations and different approaches are optimized for different applications. Interfacial coacervation or polymerization only works for a very limited range of polymers with specific solubility. Moreover, the microcapsules obtained by interfacial coacervation have thin shells, which are rather brittle. Interfacial polymerization gives more robust shells, but the reaction

conditions, such as heating, may decompose the active material in the capsule, and the unreacted monomer may remain in the core as an impurity. The solid template-based methods involve removal of the templates, which represents an extra processing step and requires the separate production of the templates. Encapsulation is then achieved by swelling of the polymer shell and diffusion of cargoes into the pre-formed microcapsules, which can have low efficiency. The double-emulsion method needs a two-step emulsification process, and each double-emulsion droplet can encompass different numbers of small droplets with different size, resulting in ill-defined morphology and heterogeneous shell thickness. Uniform double emulsions can be achieved by microfluidics,^{11, 19, 21} however, the size of capsules has to date been limited to tens of microns. Many of these problems can be overcome by the phase separation method in which microcapsules are formed by evaporation of the solvent in the discrete phase of an emulsion, under ambient conditions.^{7, 13, 33, 35} In the approach we adopt here, an oil-in-water (o/w) single emulsion contains a mixture of a polymer and a non-volatile poor solvent dissolved in a volatile good solvent as the dispersed phase. Vincent and coworkers have shown that, as the good solvent evaporates, the polymer forms small polymer-rich droplets in which the polymer phase-separates from the poor solvent (which is less volatile than the good solvent).²⁶ If the spreading coefficient and Hamaker constant have the correct sign, these polymer droplets migrate to the oil–water interface where they form a wetting film. Further evaporation of the good solvent encourages more polymer to precipitate to form a shell at the interface. High encapsulation efficiency is achieved by pre-dissolving the cargo in the volatile solvent and choosing a co-solvent that is a good solvent for the cargo but a poor solvent for the polymer. The size and shell thickness of the microcapsules is controlled by variation of the initial size of droplets and the polymer concentration.

Loss of cargo is unavoidable during storage and transport of pre-produced microcapsules,

especially in the cases where the loading or release mechanism is via swelling of the polymer shell. In-situ formation of microcapsules at a targeted location avoids loss of cargo during transportation and storage. In principle, the evaporation-driven phase separation method permits the direct formation of microcapsules on surfaces, which is of interest for applications such as pesticides, fragrances, topical medicine, and functional patterns. Therefore, developing methods for combining evaporation-driven phase separation with printing, spraying or coating technology may provide new ways for encapsulation, delivery and release.



Scheme 1. Schematic diagram of the fabrication of polymer micro-capsules by ink-jet printing.

Here we demonstrate that in-situ rapid encapsulation on targeted sites is achievable by combining ink-jet printing³⁶⁻⁴⁰ with evaporation-driven phase separation (**Scheme 1**). Ink-jet printing possesses attractive features as a manufacturing technology including efficient use of materials, scalability, patterning and localised delivery to specific locations on a surface. We have recently introduced the method of combining ink-jet printing with emulsion-solvent evaporation to generate polymeric micro-spheres on a surface.⁴¹ The challenge in producing microcapsules (rather than solid particles) lies in the short timescales of evaporation of droplets in water (the continuous phase) in the inkjet regime (~2 s). We show that phase-separation-induced microcapsule formation can indeed be achieved in inkjet printing and that a cargo initially

dissolved in the oil phase does reside within the printed capsules.

EXPERIMENTAL SECTION

Materials. Polystyrene (PS, M.W. ca. 35 kg mol⁻¹), poly(L-lactide) 2-hydroxyethyl methacrylate terminated (PLLA, M_n = 5.5 kg mol⁻¹, PDI ≤ 1.2), sodium dodecyl sulfate (SDS, > 99%), and hexamethyldisilazane (HMDS, 98%) were purchased from Sigma-Aldrich; poly(methylmethacrylate) (PMMA, M.W. ca. 35 kg mol⁻¹), poly(vinyl alcohol) (PVA, M.W. 31–50 kg mol⁻¹, 87–89% hydrolysed), Nile Red (99%) and 7,7,8,8-tetracyanoquinodimethane (TCNQ, 98%) from Acros Organics; 4-heptanone (89%) from Alfa Aesar; dichloromethane (DCM, >99%) and ethyl acetate (EtOAc, >99.99%) from Fisher Scientific; hexadecane (>98%) from TCI; tebuconazole from LKT Laboratories. All chemicals were used as received.

Preparation of emulsion. DCM solution containing polymer (e.g., 10 mg mL⁻¹ PS) and poor solvent (e.g. 1.0 v/v % hexadecane) was used as the oil phase. 0.3 wt.% PVA solution was used as the aqueous phase. The mixture of the oil phase (1.0 mL) and water phase (2.0 mL) in a 10-mL vial was then emulsified by high-speed shearing (25.9k rpm) for 30 s using a homogenizer (T10 Ultra Turrax, IKA). The emulsion obtained was sealed and kept at room temperature.

Preparation of uniform emulsion by microfluidics. Oil and water solutions were filtered through 0.2-μm PTFE filters and loaded into gas-tight borosilicate syringes. The solutions were injected by syringe pumps into a microfluidic chip (Dolomite) with a flow-focusing junction (5-μm etch depth and 8-μm junction width). The oil phase was injected into the central channel of the microfluidic chip, and the water phase into the two side channels of the microfluidic chip. The flow rate of the aqueous phase was 2 μL min⁻¹ and the flow rate of the oil phase was 0.2 μL /min. The emulsion droplet diameter was 6 μm. The emulsion thus formed was transferred via FEP

tubing to the inkjet printhead. For full experimental details, see Ref.42⁴².

Modification of substrates. Glass cover slips (22×22 mm) were first washed with ethanol, then placed in a bath sonicator in a 2 wt.% alkaline detergent solution (Decon 90; Decon Laboratories) for 30 mins, rinsed with deionized water and dried under a nitrogen flow. The cover slips were then exposed to an air plasma for 15 mins, rinsed with deionized water, dried under a nitrogen flow and placed in an oven at 70 °C for 2 h. HMDS was deposited on the surface by vapor deposition in a vacuum desiccator for 2 h. The coated cover slips were rinsed with acetone and water, and dried under a nitrogen flow.

Ink-jet printing. The ink (emulsion) was shaken well before printing. Picolitre drops of the emulsion were ejected from a Microfab drop-on-demand device (MJ-ABP-01, Microfab Technologies; 50- μm diameter orifice) controlled by a Microfab driver unit (Microfab JetDrive III Controller CT-M3-02) onto the modified substrate. The waveform used for printing was adjusted between ± 30 –40 V. The printed drops were allowed to dry freely under ambient conditions at a temperature of 20–22 °C and relative humidity of 24–50%. The evaporation process on the substrate was recorded with a high-speed camera (Photron APX RS).

Characterization. SEM images were recorded using a Hitachi SU70 SEM operated at an acceleration voltage of 5–10 kV. A conductive film of gold was coated onto the samples by sputtering before SEM imaging. The contact angle and interfacial tension (by pendent drop method) were measured by a tensiometer (FTÅ200, First Ten Ångstroms) with built-in software (Fta32 v2.0). Rheological data were collected at 293 K using an AR 2000 rheometer (TA Instruments) with a cone (2° angle) and plate geometry for PVA and SDS aqueous solutions. The steady-state viscosity of each fluid was recorded over shear rates from 0.1 to 1000 s^{-1} . The viscosity data at

shear rate 100 s^{-1} is selected because this shear rate is characteristic of the internal flows in drying droplets. Raman spectra and Raman images were recorded using a 532 nm laser (Opus 532, Laser Quantum, Manchester). Samples for Raman analysis were printed onto clean silicon substrates, and the Raman instrument was calibrated using the silicon band at 520.7 cm^{-1} . Reference spectra of polymers, tebuconazole and PVA were collected from 600 to 4000 cm^{-1} . Raman images were acquired for 30 s per image through a tuneable band-pass filter, with a 30-s acquisition time and a central Stokes shift of 2900 cm^{-1} . Data at five different filter angles were collected and used to reconstruct maps of component distribution using in-house MATLAB software. Fluorescence microscopy images was recorded using a Leica SB5 II Confocal Microscopy with PhMoNa super resolution module⁴³ using 442 nm and 532 nm excitation for TCNQ and Nile Red, respectively.

Results and Discussion

The strategy for forming microcapsules requires an oil phase predominantly formed of a good solvent for the polymer with a small amount of a solvent that is miscible with the good solvent but that is a poor solvent for the polymer. The solubility of a polymer in a solvent can be predicted from the Flory–Huggins interaction parameters of solvent–polymer pairs (χ_{S-P}),⁴⁴

$$\chi_{S-P} = \frac{V_S(\delta_S - \delta_P)^2}{RT} + 0.34 \quad [\text{Equation 1}]$$

where V_S is the molar volume of the solvent, δ_S and δ_P the solubility parameters of solvent and polymer, respectively (Table 1), R the ideal gas constant, and T the temperature. Complete solvent–polymer (S-P) miscibility is expected when $\chi_{S-P} < 0.5$, so we chose DCM as the good solvent with hexadecane as the poor solvent. The good solvent, DCM, was chosen to be much more volatile than water in order to generate polymeric particles⁴¹ rather than a continuous film⁴⁵ after evaporation. The poor solvent was chosen to be much less volatile than water so that it remained in the core of the microcapsules after the continuous phase of the droplet had dried.

Table 1. Properties of polymers and solvents.

Polymers/ Solvents	δ^a (MPa ^{1/2})	S-P	χ_{S-P}
PS	18.6	DCM-PS	0.38
PMMA	19.4	Hexadecane-PS	0.92
PLLA	21.7 ^b	DCM-PMMA	0.34
DCM	19.8	Hexadecane-PMMA	1.42
EtOAc	18.6	DCM-PLLA	0.43
Hexadecane	16.4	Hexadecane-PLLA	3.70

^a data from reference⁴⁴; ^b data from reference⁴⁶

Figure 1 shows the particles or capsules formed from an o/w emulsion as the ink, in which the oil droplets contained 10 mg mL⁻¹ PS as the shell-forming polymer and varying amounts of the core-forming poor solvent (hexadecane). The continuous phase was an aqueous solution of the emulsifier PVA. The ink was jetted through a print nozzle with a 50- μ m diameter orifice onto a transparent glass substrate modified by HMDS (water contact angle, $\theta_{\text{H}_2\text{O}} = 60 \pm 3^\circ$) and allowed to evaporate under ambient conditions. The morphology of the particles formed in-situ was observed by SEM on the dry deposit. As previously reported,⁴¹ solid PS micro-spheres are generated in the absence of hexadecane (Figure 1a₃). In the presence of 1% v/v hexadecane in DCM, porous particles were observed (Figure 1b₃), which can be attributed to the formation of droplets of hexadecane and the subsequent evaporation of hexadecane in the high-vacuum environment during SEM imaging. The particle structure involving multiple small droplets of hexadecane embedded in a PS matrix is known as occluded morphology.⁴⁰ The occluded morphology results from incomplete phase separation between shell and core. Dowding et al.⁴⁷ constructed a phase diagram for PS(MW ca. 280 kg mol⁻¹)/hexadecane/DCM mixtures; while the polymer chain length is higher than that used here, it provides an approximate model for our

experiments. For our initial composition of 0.58% hexadecane, 0.75% PS, 98.67% DCM by weight, the phase boundary is reached at 80% DCM, corresponding to a radius of droplet that is 40% of its initial size. The phase boundary is at the polymer-rich side of the two phase-region so hexadecane-rich droplets should nucleate in a continuous PS-rich phase. The low viscosity of hexadecane-rich droplets should nucleate in a continuous PS-rich phase. The low viscosity of DCM ($\mu = 0.43 \text{ mPa s}$) and low molecular weight of the PS (35 kg mol^{-1}) result in a Peclet number, $Pe < 1$ ($Pe = Ea / D \sim 0.2$, where the evaporation rate $E \sim 3 \text{ } \mu\text{m s}^{-1}$, typical droplet radius $a \sim 6 \text{ } \mu\text{m}$, and diffusion coefficient $D \sim 10^{-10} \text{ m s}^{-2}$); Pe for hexadecane is an order of magnitude

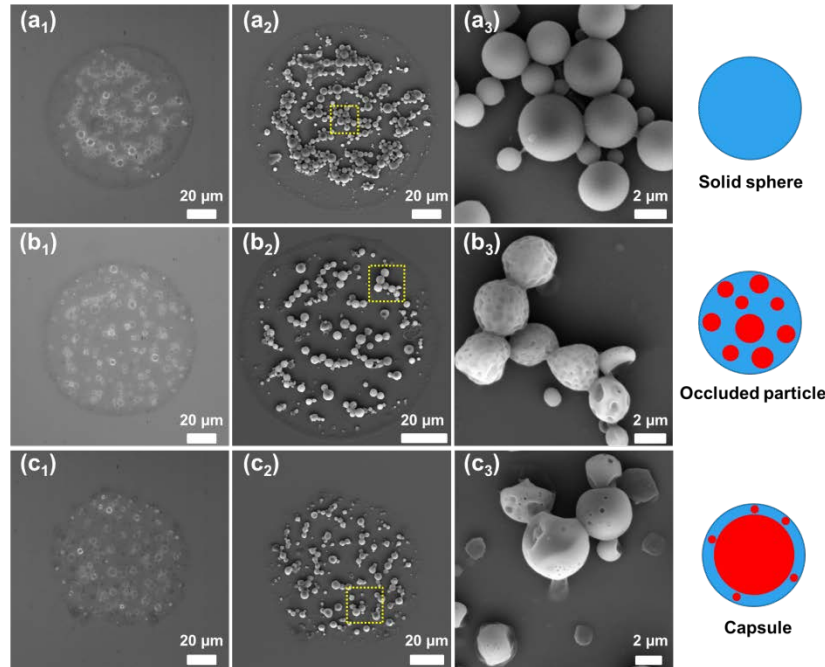


Figure 1. Morphology of PS/hexadecane particles. (a_1 , b_1 , and c_1) Micrographs and (a_2 , b_2 , and c_2) SEM images of the deposits from printed drops of emulsion containing 0.75 wt.% PS and varied hexadecane: (a) without hexadecane, (b) 0.58 wt.%, and (c) 1.16 wt.%. (a_3 , b_3 , and c_3) SEM images at high magnification showing the morphologies of the particles and corresponding schematic diagrams on the right side, where blue represents PS and red represents hexadecane.

smaller. The Peclet number^{48, 49} is a measure of the relative importance of convection and diffusion: a value of $Pe < 1$ implies that the polymer and hexadecane concentrations are approximately uniform throughout the droplets. Consequently, it is physically reasonable that nucleation of hexadecane droplets occurs within the body of the emulsion droplets, which has been observed in bigger droplets.⁵⁰ Increasing the ratio of hexadecane/PS causes the phase separation to occur earlier during drying and the hexadecane droplets coalesce more easily at higher hexadecane concentration. Indeed, particles with fewer but larger caps or even complete capsules were observed when the content of hexadecane was increased to 1.16 wt.% (Figure 1c₃).

Complete phase separation of the polymer and poor solvent does not guarantee a core-shell structure: there are three equilibrium morphologies – core-shell, acorn-like and two separated spheres, depending on the interfacial tensions (γ) of the three phases (polymer, the poor solvent, and the aqueous phase).¹³ Furthermore, either the poor solvent or the polymer could form the core. To ensure that the core contains the poor solvent, the interfacial tension of the poor solvent with the aqueous phase γ_{ow} (in the presence of emulsifier) should be higher than that between the polymer and the aqueous phase. The interfacial tension γ_{ow} depends on the emulsifier. The hexadecane/PS system can form core-shell structures with PVA ($\gamma_{ow} = 16.4 \text{ mN m}^{-1}$) as the surfactant; however, a small molecular surfactant, such as SDS, yields acorns but not exclude two separated spheres (Figure S1). SDS at a concentration of 3 mg mL^{-1} reduces the interfacial tension too much ($\gamma_{ow} = 6.7 \text{ mN m}^{-1}$), which drives hexadecane to the surface of droplets. Another advantage of using PVA is that the particles were generally observed to be randomly distributed in the deposit without either a ring stain or a central aggregate. We surmise that the PVA acts to bind the capsules to the substrate. In comparison, the particles deposited from an SDS-stabilized

emulsion were concentrated in the centre of the deposit (Figure S1) due to inward capillary forces in the latter stages of drying.⁴¹

The Hamaker constant, A_H , determines the long-range interactions between the water and oil phases separated by the polymer shell. The free energy, $F(d)$ per unit area of the water/core/shell structure is given by

$$F(d) = \gamma_{pw} + \gamma_{po} - A_H / 12\pi d^2 \quad \text{[Equation 2]}$$

where d is the thickness of the shell and γ_{pw} and γ_{po} are the polymer–water and polymer–oil interfacial tensions. If $A_H > 0$, it is favourable for the polymer shell to thin in one location and to thicken in another, giving an acorn structure with a low but finite contact angle: this situation is known as pseudo-partial wetting.⁵¹ If $A_H < 0$, then a shell of uniform d is favoured. For non-polar oils, the dominant contribution to A_H arises from high-frequency fluctuations in the electron distribution and is related to the refractive index of material. Broadly, A_H will be positive if the shell has a refractive index greater than the core and negative if the refractive index is less than the core. Since PS has a refractive index higher than both DCM and hexadecane, it is likely that $A_H > 0$ and that a core-shell structure of uniform thickness is not thermodynamically stable. This argument may explain why some open structures are observed.

The method for in-situ production of microcapsules can be extended to other polymers and oils that have appropriate interaction parameters (Table 1) and interfacial properties (Table 2). Water-insoluble polymers with higher values of δ are predicted to form core-shell structures, because a higher δ results in poorer compatibility with hexadecane, which favors phase separation, and greater hydrophilicity, which preferentially localises the polymer at the oil/water interface. The experimental contact angles θ and interfacial tensions γ_{ow} between the three phases are shown in Table 2. The contact angle refers to the liquid drop (the poor solvents or the aqueous phase) on the

polymer film in air. The polymer films were prepared by evaporation of 20 mg mL⁻¹ DCM solutions containing corresponding polymers (PS, PMMA, or PLLA) on the substrate. Both PMMA and PLLA form microcapsules rather than occluded particles (Figure S2), which can be explained by the compatibility of polymer and hexadecane judged by χ_{S-P} (PLLA > PMMA > PS) and γ_{op} (PLLA > PMMA > PS).

Table 2. Contact angles or interfacial tensions of the three phases.

Phase <i>o</i>	Phase <i>w</i>	Phase <i>p</i>	θ_{op} (°)	θ_{pw} (°)	γ_{ow} (mN m ⁻¹)
Hexadecane	3 mg mL ⁻¹ PVA	PS	6.35	69.7	16.4
Hexadecane	3 mg mL ⁻¹ PVA	PMMA	15.3	70.5	16.4
Hexadecane	3 mg mL ⁻¹ PVA	PLLA	28.4	60.9	16.4
4-heptanone & sunflower oil	3 mg mL ⁻¹ PVA	PS	21.8	69.7	11.0
4-heptanone & sunflower oil	3 mg mL ⁻¹ PVA	PMMA	12.6	70.5	11.0
4-heptanone & sunflower oil	3 mg mL ⁻¹ PVA	PLLA	24.2	60.9	11.0

DCM can be replaced by other volatile solvents. In laboratory studies, DCM is commonly employed because it is a good solvent for many polymers, is immiscible with water and evaporates readily (which requires both a high vapour pressure and sufficient solubility in water that diffusion through the continuous phase is not rate-limiting). However, exposure to DCM vapor at high levels is hazardous to the health and there are increasing restrictions on the release of DCM into the environment. Safer and more environmentally friendly solvents should share the favourable physical properties of DCM, in terms of solubility for polymers and cargoes, immiscibility with

water, and volatility. Ethyl acetate (EtOAc) is a low-toxicity solvent that generally meets these conditions. Microcapsules of both PS ($\chi_{EtOAc-PS} = 0.34$) and PMMA ($\chi_{EtOAc-PMMA} = 0.37$) were obtained with EtOAc instead of DCM (Figure 2). The microcapsules prepared with EtOAc (diameter $< 2.0 \mu\text{m}$) were smaller than those produced with DCM, because the lower interfacial tension between the oil phase and the aqueous phase leads to smaller emulsion droplets ($\gamma_{ow} = 3.2 \text{ mN m}^{-1}$ with EtOAc compared to $\gamma_{ow} = 8.0 \text{ mN m}^{-1}$ with DCM). EtOAc is not a good solvent for PLLA, as predicted from the value of $\chi_{EtOAc-PLLA} = 0.72$.

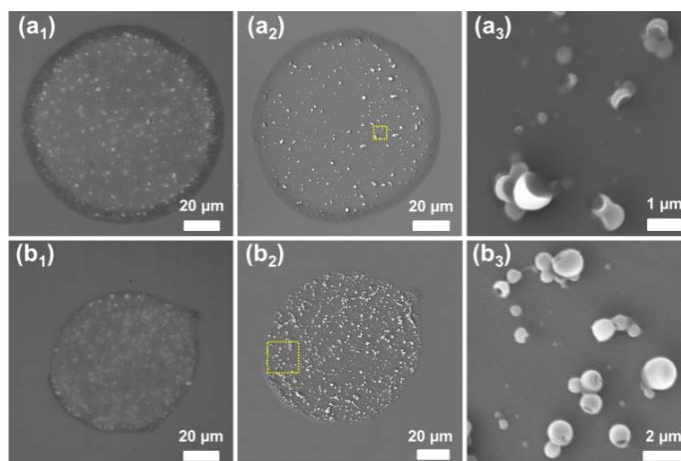


Figure 2. (a) PS and (b) PMMA microcapsules prepared with EtOAc as the good solvent. Micrographs (a₁ and b₁) and SEM images (a₂ and b₂) of the deposits from printed emulsion drops; (a₃ and b₃): SEM images at high magnification showing the morphologies of the microcapsules.

Hexadecane has two disadvantages as a core-forming solvent: (i) its high melting point (18 °C) can lead to freezing at low temperatures, reducing release rates and potentially rupturing capsules; (ii) it is a poor solvent for functional cargoes that are polar. An alternative core-forming solvent with higher polarity is 4-heptanone.⁴⁷ Heptanone still has appreciable volatility (normal boiling point is 144 °C), so we used a mixture of 4-heptanone with a polar oil (sunflower oil) to prevent collapse of the capsules as the heptanone diffuses through the shell and evaporates. The formation

of well-defined PS, PMMA and PLLA microcapsules with 4-heptanone/sunflower oil core was confirmed by SEM (Figure 3).

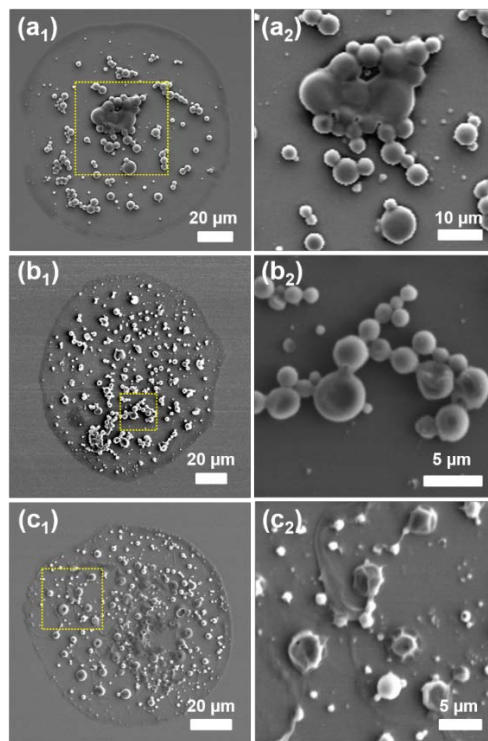


Figure 3. (a) PS, (b) PMMA, and (c) PLLA microcapsules prepared with 4-heptanone/sunflower oil mixture as the core-forming oil. (a₁, b₁ and c₁) SEM images of the deposits from printed emulsion drops. (a₂, b₂ and c₂) SEM images at high magnification showing the morphologies of the microcapsules.

To confirm that the oil is retained within the micro-capsules, we dissolved fluorescent dyes in the oil phase of the emulsions and imaged the dry deposits. Figure 4 shows examples of microcapsules with shells of PS or PMMA, hexadecane or heptanone/sunflower oil as the poor solvent, and Nile Red or TCNQ as the dye. In each case there is good overlap of the optical micrograph and confocal fluorescence micrograph, showing that dye molecules are confined in the oil core of the micro-capsules. No significant fluorescence was observed from the regions outside

of the microcapsules indicating a high degree of encapsulation.

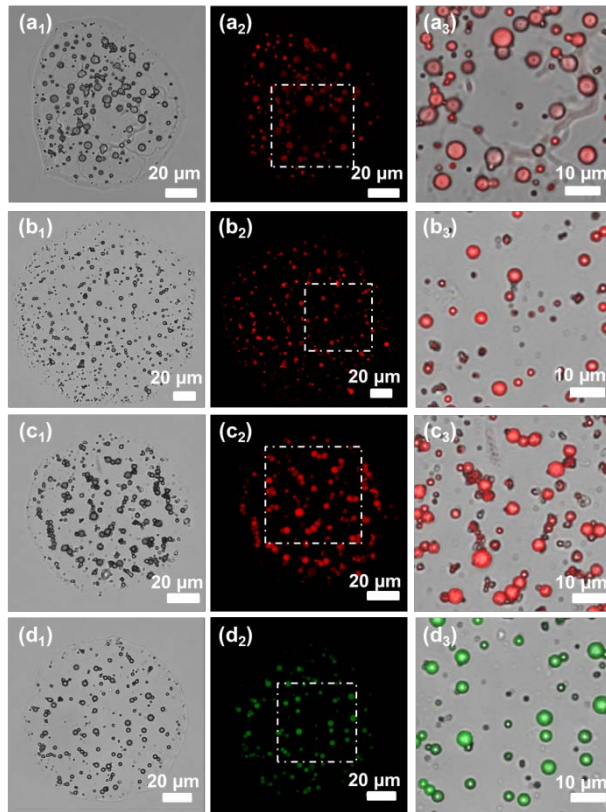


Figure 4. Encapsulation of dyes into polymeric micro-capsules: (a) PS shell + heptanone/sunflower oil core with Nile red, (b) PMMA shell + heptanone/sunflower oil core with Nile Red, (c) PMMA shell + hexadecane core with Nile Red, (d) PMMA shell + heptanone/sunflower oil core with TCNQ. Left column: bright-field images; middle column: confocal fluorescence microscopy images; right column: overlaid optical and fluorescence images of selected regions.

The time for formation of microcapsules (< 5 s) in printed droplets is much shorter than in microcapsules formed by bulk evaporation (tens of minutes or longer).⁵⁰ The evaporation of a representative drop is shown in Figure 5. Most oil droplets evaporated within 2 s to give a particulate dispersion rather than an emulsion. At this point the level of the continuous phase is higher than the particles, which remain fully immersed in the fluid. After 3 s, the level of the water

dropped below the largest particles whose capsule structure is clearly seen as a bright ring in transmitted light. After 4 s, the water has nearly fully evaporated. The evaporation of the solvent of the dispersed phase (DCM) before the continuous phase (water) prevents coalescence of the droplets and yields discrete particles/capsules rather than a continuous film.

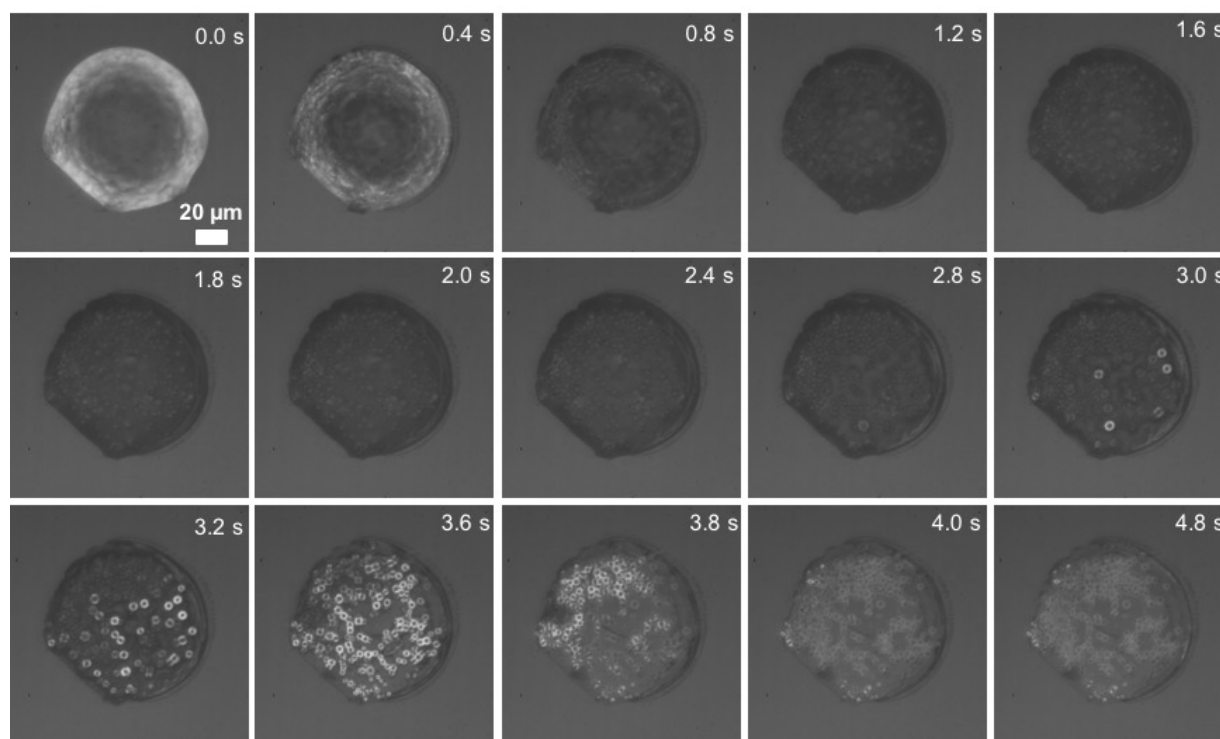


Figure 5. Micrographs of the evolution of a printed emulsion drop on the substrate during evaporation.

For practical applications we need to be able to load functional cargoes into polymer particles or microcapsules produced by printing or spraying of emulsions. As a demonstration system, we chose the fungicide tebuconazole, which inhibits the biosynthesis of ergosterols in fungi and which is used for treatment of seeds and spraying of commercial crops. Tebuconazole breaks down slowly in the environment and is toxic to aquatic life. Encapsulation of tebuconazole by polymer could be useful for delayed or triggered release on leaf surfaces and might also reduce animal

toxicity because of slow release *in vivo*.

We initially explored the printing of solid polymer particles containing tebuconazole. The miscibility of polymers and small molecular cargoes can be predicted via the solubility parameter. The solubility parameter of tebuconazole ($\delta = 20.4 \text{ MPa}^{1/2}$) was calculated from group contributions (Equation 3):⁵²

$$\delta = \sqrt{\delta_d^2 + \delta_p^2 + \delta_h^2} \quad [\text{Equation 3}]$$

where δ_d , δ_p , and δ_h , represent contributions from dispersion forces, dipole–dipole interactions, and hydrogen bonding, respectively. Tebuconazole is predicted to mix well with PMMA or PLLA because the difference in solubility parameters $\Delta\delta < 2 \text{ MPa}^{1/2}$. Figure 6 shows particles of PMMA or PLLA with tebuconazole in a 1:1 mass ratio. No tebuconazole crystals were observed under crossed polarizers indicating that the active ingredient remained dissolved within the polymer matrix.

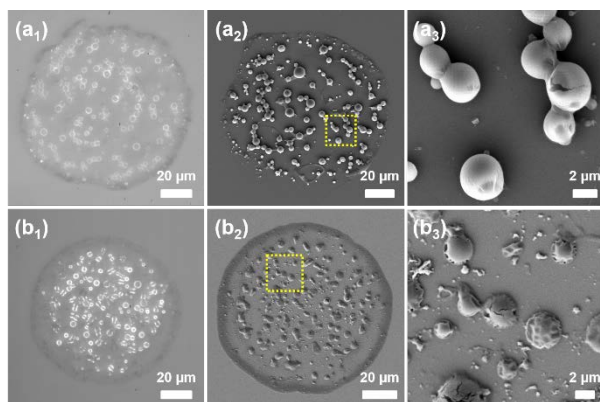


Figure 6. Encapsulation of tebuconazole into polymeric particles: (a) PMMA and (b) PLLA. (a₁ and b₁) Micrographs and (a₂ and b₂) SEM images of the deposits from printed drops of emulsion containing 1:1 tebuconazole and polymers. (a₃ and b₃) SEM images at high magnification showing the morphologies of the particles.

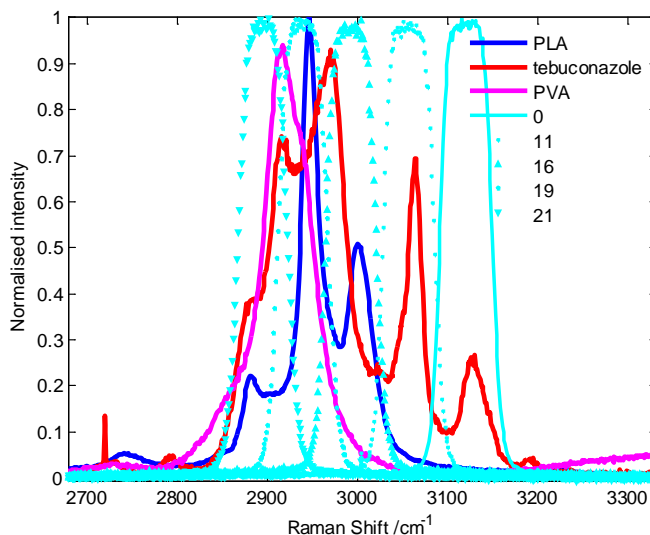


Figure 7. Raman spectra of PLLA, tebuconazole, PVA and transmission profiles normalised to the maximum transmission at the filter angles of 0°, 11°, 16°, 19° and 21° used in the fitting procedure.

Raman imaging confirms that the tebuconazole is distributed within the polymer particles. The spatial resolution of the Raman images is $\sim 1 \mu\text{m}$, which is sufficient to determine if phase separation has occurred. Figure 7 shows the Raman spectra of PLLA, tebuconazole, and PVA in the C–H stretching region (2800 to 3200 cm^{-1}). Images of the sample were acquired through a tuneable filter for different filter angles which cover the characteristic peaks of the three components in the dry deposits. Five filter angles are sufficient to deconvolute the overlapping features in the different spectral windows and to recover images of the three components, which are shown in Figure 8. The maps of PLLA and tebuconazole superimpose showing that tebuconazole is dispersed throughout PLLA matrix without phase separation. A weak signal from the PVA is observed around the particles, identifying the thin film covering the droplet footprint in optical micrographs as PVA. No tebuconazole is observed outside of the polymer particles as expected from its extremely low solubility in water (0.032 mg mL^{-1}) and high solubility in DCM

(>200 mg mL⁻¹). A similar result was also obtained when PLLA was replaced by PS (Figure S3) or PMMA (Figure S4).

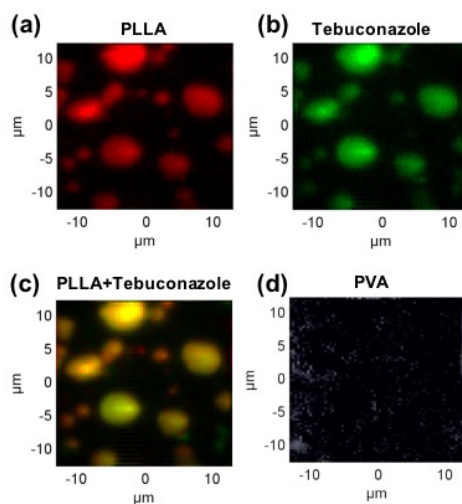


Figure 8. Reconstructed Raman images of components of particles containing 1/1 tebuconazole and PLLA from partial region of a printed deposit (a) PLLA, (b) tebuconazole, (c) PLLA + tebuconazole, and (d) PVA.

Cargoes dispersed throughout the polymer matrix of a solid particles have potential for sustained release (e.g. of biocides). For the purpose of controlled release, it is better to load the cargoes into the core of microcapsules, where the shell thickness can be used to vary the release rate and the shell permeability can be tuned to vary with environmental conditions. Additionally, for our agrochemical model system an oleophilic adjuvant is necessary to enhance transport across the cuticle of a leaf: this adjuvant could also be encapsulated in the core of the microcapsule. The core-forming oil should be a good solvent for cargoes so that the cargo remains dissolved in the core when the polymer shell phase-separates. For tebuconazole, we selected the 4-heptanone/sunflower oil mixture as the core-forming oil and the biodegradable polymer PLLA for the shell. Microcapsules loaded with tebuconazole were obtained by the emulsion-solvent evaporation

technique (Figure 9a). After 3 weeks, most microcapsules degraded under ambient conditions (Figure 9b), releasing puddles of sunflower oil and tebuconazole. In principle, the shell thickness of microcapsules can be controlled by varying the ratio of polymer/poor solvent,⁴⁷ which in turn affects the degradation time and thus the release rate of cargoes.

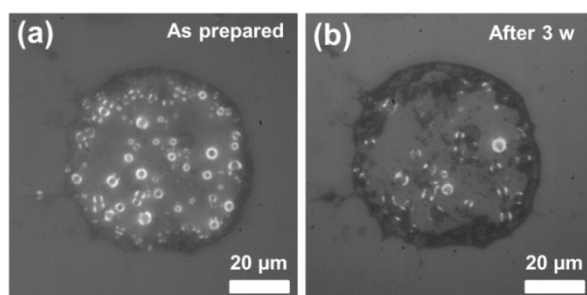


Figure 9. Encapsulation of tebuconazole into PLLA microcapsules: Micrographs of a deposit as prepared (a) and after 3 weeks (b).

To develop the experimental conditions for the successful production of microcapsules by inkjet printing we used homogenized emulsions with a high degree of polydispersity and hence obtained capsules with a large range of sizes. Since the size of microcapsules is an important parameter that affects their properties, it is desirable to control the microcapsule size within a narrower size range. Uniform emulsion droplets can be produced by microfluidics²¹ or membrane emulsification.⁵³ We have chosen the former approach and used a flow-focussing junction to produce monodisperse emulsion droplets with a diameter of 7 μm. The emulsion was then printed through an 80-μm nozzle to reduce the shear rates that cause fission of emulsion droplets. Supplementary Video S1 shows the drying of an emulsion droplet and the conversion of oil droplets to capsules. Figure 10a shows an SEM image of a dry deposit showing a single layer of capsules with a PMMA shell and a hexadecane core. The size distribution of the capsules (see high-resolution SEM image in Figure 10b) is much narrower than from the homogenized emulsion,

but broader than size distribution of the emulsion drops before printing due to some coalescence/break-up during the printing process.⁴²

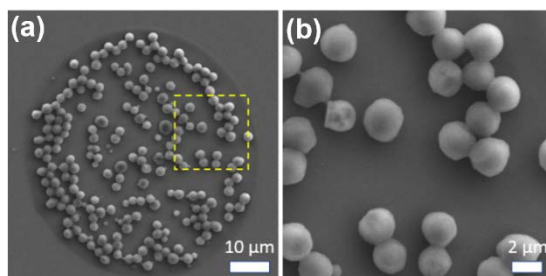


Figure 10. (a) SEM image of the deposit formed by inkjet printing of a monodisperse emulsion produced from a continuous phase of 0.3 wt% PVA in water and a discrete phase comprising 1.6 wt% PMMA and 0.9 wt% hexadecane in DCM onto a HDMS treated glass slide. (b) High-magnification SEM showing the morphologies and size distribution of the microcapsules.

Conclusion

We have demonstrated a method for rapid encapsulation of cargoes into polymeric microcapsules via ink-jet printing of emulsions. Evaporation of the good solvent induced phase separation between the polymer and the non-volatile poor solvent within seconds, resulting in the formation of microcapsules with a polymer shell and liquid core. The interactions between the good solvent, the poor solvent, the polymer, and the aqueous phase play key roles in the morphology of particles. Fluorescent dyes were used to show that the core-forming oil is retained within the capsules. Raman imaging showed that a model active ingredient (the fungicide tebuconazole) can be encapsulated within solid polymer spheres without phase separation. Microcapsules containing tebuconazole dissolved in 4-heptanone/sunflower oil were also produced. High loadings and encapsulation efficiencies can be achieved for cargoes that possess high miscibility with polymers or the oil core but poor solubility in the aqueous phase. The good solvent of the oil phase, dichloromethane, can be replaced by low toxicity solvents such as ethylacetate for polymers and

cargoes with appropriate solubility parameters. This versatile method for in-situ and rapid encapsulation may be useful for applications in precision spraying of pesticides, dermatological treatment, fragrances, functional graphics and coatings.

ASSOCIATED CONTENT

Supporting Information.

Supporting information including additional figures and a video. The following file is available free of charge via the Internet at <http://pubs.acs.org>.

Additional figures (PDF) and a video (AVI)

AUTHOR INFORMATION

Corresponding Authors

*E-mail: c.d.bain@durham.ac.uk; rhd.deng@gmail.com

Notes

The authors declare no competing financial interest.

ACKNOWLEDGMENT

The authors are grateful to M. Possiwan and A. Piñeiro Romero for Raman imaging and Dr. R. Pal for fluorescence microscopy imaging. The code to analyse Raman images was written by M. Possiwan and Dr. L. Yang. This work was funded by the EPSRC under Grant EP/N025245/1. YW thanks Durham University and the China Scholarship Council for studentship funding.

REFERENCES

1. White, S. R.; Sottos, N. R.; Geubelle, P. H.; Moore, J. S.; Kessler, M. R.; Sriram, S. R.; Brown, E. N.; Viswanathan, S., Autonomic Healing of Polymer Composites. *Nature* **2001**, *409*, 794.
2. Zhao, Y.; Fickert, J.; Landfester, K.; Crespy, D., Encapsulation of Self-Healing Agents in Polymer Nanocapsules. *Small* **2012**, *8*, 2954-2958.
3. Kim, S.-R.; Getachew, B. A.; Park, S.-J.; Kwon, O.-S.; Ryu, W.-H.; Taylor, A. D.; Bae, J.; Kim, J.-H., Toward Microcapsule-Embedded Self-Healing Membranes. *Environ. Sci. Technol. Lett.* **2016**, *3*, 216-221.
4. Geng, J.; Li, W.; Smaga, L. P.; Sottos, N. R.; Chan, J., Damage-Responsive Microcapsules for Amplified Photoacoustic Detection of Microcracks in Polymers. *Chem. Mater.* **2018**, *30*, 2198-2202.
5. Li, W.; Matthews, C. C.; Yang, K.; Odarczenko, M. T.; White, S. R.; Sottos, N. R., Autonomous Indication of Mechanical Damage in Polymeric Coatings. *Adv. Mater.* **2016**, *28*, 2189-2194.
6. Yoo, Y.; Martinez, C.; Youngblood, J. P., Synthesis and Characterization of Microencapsulated Phase Change Materials with Poly(urea-urethane) Shells Containing Cellulose Nanocrystals. *ACS Appl. Mater. Interfaces* **2017**, *9*, 31763-31776.
7. Xu, J.; Li, J.; Yang, Y.; Wang, K.; Xu, N.; Li, J.; Liang, R.; Shen, L.; Xie, X.; Tao, J.; Zhu, J., Block Copolymer Capsules with Structure-Dependent Release Behavior. *Angew. Chem. Int. Ed.* **2016**, *55*, 14633-14637.

8. Liu, J. W.; Zhang, Y.; Wang, C. Y.; Xu, R. Z.; Chen, Z. P.; Gu, N., Magnetically Sensitive Alginate-Templated Polyelectrolyte Multilayer Microcapsules for Controlled Release of Doxorubicin. *J. Phys. Chem. C* **2010**, *114*, 7673-7679.
9. Xia, Y.; Wu, J.; Du, Y.; Miao, C.; Su, Z.; Ma, G., Bridging Systemic Immunity with Gastrointestinal Immune Responses via Oil-in-Polymer Capsules. *Adv. Mater.* **2018**, e1801067.
10. Fenton, O. S.; Olafson, K. N.; Pillai, P. S.; Mitchell, M. J.; Langer, R., Advances in Biomaterials for Drug Delivery. *Adv. Mater.* **2018**, e1705328.
11. Zhang, L.; Cai, L. H.; Lienemann, P. S.; Rossow, T.; Polenz, I.; Vallmajo-Martin, Q.; Ehrbar, M.; Na, H.; Mooney, D. J.; Weitz, D. A., One-Step Microfluidic Fabrication of Polyelectrolyte Microcapsules in Aqueous Conditions for Protein Release. *Angew. Chem. Int. Ed.* **2016**, *55*, 13470-13474.
12. Ravanfar, R.; Celli, G. B.; Abbaspourrad, A., Controlling the Release from Enzyme-Responsive Microcapsules with A Smart Natural Shell. *ACS Appl. Mater. Interfaces* **2018**, *10*, 6046-6053.
13. Pekarek, K. J.; Jacob, J. S.; Mathiowitz, E., Double-Walled Polymer Microspheres for Controlled Drug Release. *Nature* **1994**, *367*, 258-260.
14. ten Cate, A. T.; Gaspar, C. H.; Virtanen, H. L. K.; Stevens, R. S. A.; Koldewey, R. B. J.; Olkkonen, J. T.; Rentrop, C. H. A.; Smolander, M. H., Printed Electronic Switch on Flexible Substrates Using Printed Microcapsules. *J. Mater. Sci.* **2014**, *49*, 5831-5837.
15. Rengarajan, G. T.; Walder, L.; Gorb, S. N.; Steinhart, M., High-Throughput Generation of Micropatterns of Dye-Containing Capsules Embedded in Transparent Elastomeric Monoliths by Inkjet Printing. *ACS Appl. Mater. Interfaces* **2012**, *4*, 1169-1173.

16. Kim, M.; Park, K. J.; Seok, S.; Ok, J. M.; Jung, H. T.; Choe, J.; Kim, D. H., Fabrication of Microcapsules for Dye-Doped Polymer-Dispersed Liquid Crystal-Based Smart Windows. *ACS Appl. Mater. Interfaces* **2015**, *7*, 17904-17909.
17. Guldin, S.; Kohn, P.; Stefik, M.; Song, J.; Divitini, G.; Ecarla, F.; Ducati, C.; Wiesner, U.; Steiner, U., Self-Cleaning Antireflective Optical Coatings. *Nano letters* **2013**, *13*, 5329-5335.
18. Savolainen, A.; Zhang, Y.; Rochefort, D.; Holopainen, U.; Erho, T.; Virtanen, J.; Smolander, M., Printing of Polymer Microcapsules for Enzyme Immobilization on Paper Substrate. *Biomacromolecules* **2011**, *12*, 2008-2015.
19. Lee, H.; Choi, C. H.; Abbaspourrad, A.; Wesner, C.; Caggioni, M.; Zhu, T.; Weitz, D. A., Encapsulation and Enhanced Retention of Fragrance in Polymer Microcapsules. *ACS Appl. Mater. Interfaces* **2016**, *8*, 4007-4013.
20. Amstad, E., Capsules: Their Past and Opportunities for Their Future. *ACS Macro Lett.* **2017**, *6*, 841-847.
21. Abbaspourrad, A.; Carroll, N. J.; Kim, S. H.; Weitz, D. A., Polymer Microcapsules with Programmable Active Release. *J. Am. Chem. Soc.* **2013**, *135*, 7744-7750.
22. Tang, S.; Tang, L.; Lu, X.; Liu, H.; Moore, J. S., Programmable Payload Release from Transient Polymer Microcapsules Triggered by A Specific Ion Coactivation Effect. *J. Am. Chem. Soc.* **2018**, *140*, 94-97.
23. Gun, W. J.; Routh, A. F., Formation and Characterization of pH-Responsive Liquid Core Microcapsules. *Langmuir* **2013**, *29*, 12541-12548.
24. DiLauro, A. M.; Abbaspourrad, A.; Weitz, D. A.; Phillips, S. T., Stimuli-Responsive Core-Shell Microcapsules with Tunable Rates of Release by Using A Depolymerizable Poly(phthalaldehyde) Membrane. *Macromolecules* **2013**, *46*, 3309-3313.

25. Deng, R.; Derry, M. J.; Mable, C. J.; Ning, Y.; Armes, S. P., Using Dynamic Covalent Chemistry To Drive Morphological Transitions: Controlled Release of Encapsulated Nanoparticles from Block Copolymer Vesicles. *J. Am. Chem. Soc.* **2017**, *139*, 7616-7623.
26. Dowding, P. J.; Atkin, R.; Vincent, B.; Bouillot, P., Oil Core/Polymer Shell Microcapsules by Internal Phase Separation from Emulsion Droplets. II: Controlling the Release Profile of Active Molecules. *Langmuir* **2005**, *21*, 5278-5284.
27. Wu, M.; Zhu, Y.; Jiang, W., Release Behavior of Polymeric Vesicles in Solution Controlled by External Electrostatic Field. *ACS Macro Lett.* **2016**, *5*, 1212-1216.
28. Park, C. H.; Lee, S.; Pornnoppadol, G.; Nam, Y. S.; Kim, S.-H.; Kim, B. J., Microcapsules Containing pH-Responsive, Fluorescent Polymer-Integrated MoS₂: An Effective Platform for in Situ pH Sensing and Photothermal Heating. *ACS Appl. Mater. Interfaces* **2018**, *10*, 9023-9031.
29. Cui, J.; van Koeveden, M. P.; Mullner, M.; Kempe, K.; Caruso, F., Emerging Methods for the Fabrication of Polymer Capsules. *Adv. Colloid Interface Sci.* **2014**, *207*, 14-31.
30. Yow, H. N.; Routh, A. F., Formation of Liquid Core–Polymer Shell Microcapsules. *Soft Matter* **2006**, *2*, 940-949.
31. Bouchemal, K.; Briançon, S.; Perrier, E.; Fessi, H.; Bonnet, I.; Zydowicz, N., Synthesis and Characterization of Polyurethane and Poly(ether urethane) Nanocapsules Using A New Technique of Interfacial Polycondensation Combined to Spontaneous Emulsification. *Inter. J. Pharm.* **2004**, *269*, 89-100.
32. van Zyl, A. J. P.; Sanderson, R. D.; de Wet-Roos, D.; Klumperman, B., Core/shell Particles Containing Liquid Cores: Morphology Prediction, Synthesis, and Characterization. *Macromolecules* **2003**, *36*, 8621-8629.

33. Atkin, R.; Davies, P.; Hardy, J.; Vincent, B., Preparation of Aqueous Core/Polymer Shell Microcapsules by Internal Phase Separation. *Macromolecules* **2004**, *37*, 7979-7985.
34. Yu, X.; Zhao, Z.; Nie, W.; Deng, R.; Liu, S.; Liang, R.; Zhu, J.; Ji, X., Biodegradable Polymer Microcapsules Fabrication through A Template-Free Approach. *Langmuir* **2011**, *27*, 10265-10273.
35. Loxley, A.; Vincent, B., Preparation of Poly(methylmethacrylate) Microcapsules with Liquid Cores. *J. Colloid Interface Sci.* **1998**, *208*, 49-62.
36. H. J. Spinelli, Polymeric dispersants in ink jet technology. *Adv. Mater.* **1998**, *10*, 1215.
37. H. Sirringhaus, T. Kawase, R. H. Friend, T. Shimoda, M. Inbasekaran, W. Wu, E. P. Woo, High-resolution inkjet printing of all-polymer transistor circuits. *Science* **2000**, *290*, 2123.
38. B. J. de Gans, P. C. Duineveld, U. S. Schubert, Inkjet printing of polymers: state of the art and future developments. *Adv. Mater.* **2004**, *16*, 203.
39. J. Hou, M. Li, Y. Song, Patterned colloidal photonic crystals. *Angew. Chem. Int. Ed.* **2018**, *57*, 2544.
40. M. Kuang, L. Wang, Y. Song, Controllable printing droplets for high - resolution patterns. *Adv. Mater.* **2014**, *26*, 6950-6958.
41. Deng, R.; Yang, L.; Bain, C. D., Combining Inkjet Printing with Emulsion Solvent Evaporation to Pattern Polymeric Particles. *ACS Appl. Mater. Interfaces* **2018**, *10*, 12317-12322.
42. Wang, Y.; Deng, R.; Yang, L.; Bain, C., Fabrication of Monolayers of Uniform Polymeric Particles by Inkjet Printing of Monodisperse Emulsions Produced by Microfluidics. DOI: [10.1039/C9LC00588A](https://doi.org/10.1039/C9LC00588A).
43. Pal, R., Phase Modulation Nanoscopy: A Simple Approach to Enhanced Optical Resolution. *Faraday Discuss.* **2015**, *177*, 507-515.

44. Brandrup, J., Immergut, E. H., Grulke, E. A., Eds.; , Polymer Handbook; Wiley: New York, 1999; Section VII, pp 675-714.
45. Johns, A. S.; Bain, C. D., Ink-Jet Printing of High-Molecular-Weight Polymers in Oil-in-Water Emulsions. *ACS Appl. Mater. Interfaces* **2017**, *9*, 22918-22926.
46. Agrawal, A.; Saran, A. D.; Rath, S. S.; Khanna, A., Constrained Nonlinear Optimization for Solubility Parameters of Poly(lactic acid) and Poly(glycolic acid)-Validation and Comparison. *Polymer* **2004**, *45*, 8603-8612.
47. Dowding, P. J.; Atkin, R.; Vincent, B.; Bouillot, P., Oil Core-Polymer Shell Microcapsules Prepared by Internal Phase Separation from Emulsion Droplets. I. Characterization and Release Rates for Microcapsules with Polystyrene Shells. *Langmuir* **2004**, *20*, 11374-11379.
48. Bahadur, J.; Sen, D.; Mazumder, S.; Bhattacharya, S.; Frielinghaus, H.; Goerigk G., Origin of Buckling Phenomenon during Drying of Micrometer-Sized Colloidal Droplets. *Langmuir* **2011**, *27*, 8404-8414.
49. Sen, D.; Bahadur, J.; Mazumder, S.; Santoro, G.; Yu S.; Roth, S. V., Probing Evaporation Induced Assembly Across A Drying Colloidal Droplet Using In Situ Small-Angle X-Ray Scattering at The Synchrotron Source. *Soft Matter*, **2014**,*10*, 1621-1627.
50. Liu, S.; Cai, M.; Deng, R.; Wang, J.; Liang, R.; Zhu, J., Fabrication of Porous Polymer Microparticles with Tunable Pore Size and Density through the Combination of Phase Separation and Emulsion-Solvent Evaporation Approach. *Korea-Australia Rheology J.* **2014**, *26*, 63-71.
51. Brochard-Wyart, F.; Di Meglio, J. M.; Quere, D.; De Gennes, P. G., Spreading of Nonvolatile Liquids in A Continuum Picture. *Langmuir* **1991**, *7*, 335-338.

52. Krevelen, D. W. v., Properties of Polymers: Their Estimation and Correlation with Chemical Structure. 2nd ed.; Elsevier: New York, 1976.

53. Shin, J. M.; Kim, M. P.; Yang, H.; Ku, K. H.; Jang, S. G.; Youm, K. H.; Yi, G.-R.; Kim, B. J., Monodisperse Nanostructured Spheres of Block Copolymers and Nanoparticles via Cross-Flow Membrane Emulsification. *Chem. Mater.* **2015**, 27, 6314-6321.

Table of Contents

